crystals

MDPI

Article

The Tip of Dendritic Crystal in an Inclined Viscous Flow

Ilya O. Starodumov [1,*], Ekaterina A. Titova [2], Eugeny V. Pavlyuk [3] and Dmitri V. Alexandrov [1,3]

[1] Laboratory of Multiphase Physical and Biological Media Modelling, Ural Federal University, Lenin Ave., 51, 620000 Ekaterinburg, Russia
[2] Laboratory of Mathematical Modeling of Physical and Chemical Processes in Multiphase Media, Ural Federal University, Lenin Ave., 51, 620000 Ekaterinburg, Russia
[3] Laboratory of Multi-Scale Mathematical Modeling, Department of Theoretical and Mathematical Physics, Ural Federal University, Lenin Ave., 51, 620000 Ekaterinburg, Russia
* Correspondence: ilya.starodumov@urfu.ru; Tel.: +7-343-389-9477

Abstract: We study the flow around the tip of a dendritic crystal by an inclined stream of viscous incompressible liquid. The tip shape is chosen accordingly to recent theory [*Philos. Trans. R. Soc. A* **2020**, *378*, 20190243] confirmed by a number of experiments and computations [*Philos. Trans. R. Soc. A* **2021**, *379*, 20200326]. Our simulations have been carried out for a 0, 30, 60, and 90-degree flow slope to the dendrite axis. We show that the stream inclination has a significant effect on the hydrodynamic flow and shear stress. In particular, a transition from laminar to turbulent currents on the upstream side of the dendritic crystal may occur in an inclined hydrodynamic flow. This leads to the fact that the heat and mass transfer mechanisms on the upstream and downstream sides of a growing dendritic crystal may be different.

Keywords: dendrite; inclined viscous flow; hydrodynamics

Citation: Starodumov, I.O.; Titova, E.A.; Pavlyuk, E.V.; Alexandrov, D.V. The Tip of Dendritic Crystal in an Inclined Viscous Flow. *Crystals* **2022**, *12*, 1590. https://doi.org/10.3390/cryst12111590

Academic Editor: Helmut Cölfen

Received: 7 October 2022
Accepted: 7 November 2022
Published: 8 November 2022

1. Introduction

It is well known that the dendritic form is one of the most common forms of crystals growing in supercooled melts and supersaturated solutions. As this takes place, the dendritic growth rate and the dispersion of the material microstructure are determined by heat and mass transfer processes and melt hydrodynamic currents near the liquid–solid interface. Recently a number of new theoretical results extending the understanding of dendritic crystal growth dynamics have been obtained [1–8]. Thus, the problem of stable growth of the free-growing dendrite tip as well as the problem of the influence of convective melt flow on dendrite tip growth and lateral branch formation are relevant and under active investigation [9–11]. For example, a plane-parallel flow of supercooled melt flowing around the dendrite essentially influences the characteristics of the stable mode of dendritic growth. Namely, the tip velocity of the dendritic crystal and selection parameter strongly increase with increasing hydrodynamic flow rate, while the tip radius of the crystal decreases [12,13].

Natural convection (e.g., thermogravitational in the Earth's gravity field or thermocapillary in microgravity) as well as forced convective flows of the melt (e.g., in electromagnetic levitation facilities) drastically change the mechanisms of heat and mass transfer near the interfaces of dendritic growth. Namely, convection substantially changes local temperature and impurity concentration gradients and thus changes the dynamics of interfacial crystal growth (e.g., the development of morphological instability and formation of secondary dendrite branches) [14–17]. Experimental data and theoretical estimates [18,19] as well as phase-field simulations [20–22] indicate a significant influence of fluid convection on the formation of dendritic material microstructure. So, for example, secondary dendritic branches predominantly grow on the side of the main dendrite flow, while on the opposite side they grow considerably less [22,23]. As this takes place, melt convection gives rise to

the amplitude and frequency of dendritic side branches [21]. In addition, experimental data on the cast structure of an alloy Al 99.5 solidified in the mechanical stirrer demonstrate that the grains are inclined into the upstream direction [24]. Moreover, experiments on dendritic structure of AI-4% Si alloy showed that the fluid flow modified the dendrite spacing from large passing small to large [25]. Thus, convective flow affects phase selection [26,27], grain structure refinement [28,29], and generally the formation of solid structure of crystallizing materials [30]. In addition, intense convective melt flows near interfaces may change the mechanism of heat and mass transfer, i.e., instead of conductive boundary conditions of heat and mass transfer, the corresponding convective boundary conditions take place [31–35].

Given the importance of melt flow in dendritic growth theory, in this paper we study the influence of the tilt angle on the hydrodynamic flow around a dendritic crystal. In doing so, an important feature of the study is the consideration of the real shape of the dendritic tip, recently derived analytically by Alexandrov and Galenko in Ref. [36] and then confirmed by comparing the theory with experiments and numerical simulations (using the phase-field and enthalpy methods) in Refs. [37,38].

2. The Model

Let us consider a tip region of dendritic crystal submerged into a forced convective flow of viscous fluid. In addition, we consider the case of steady-state dendritic growth in a hydrodynamic melt flow. It is well known that the growing dendritic crystal after a certain time reaches the steady-state growth scenario with the tip diameter and tip shape remaining unchanged [21–23,39–41]. Keeping this in mind, the dendrite tip shape will be considered accordingly to a recently developed theory by Alexandrov and Galenko [36]. For the sake of convenience, let us be revise the main points of this theory for a three-dimensional crystal. Let the origin of Cartesian coordinate system be at the dendritic tip. The main trunk of crystal is directed in the negative $(-z)$ direction while the x-axis touches the origin and passes in a perpendicular direction. In this case, the 3D tip shape of a dendritic crystal is given by (x and z are scaled by the dendrite tip diameter) [36]

$$z = \alpha z_{\mathrm{AG}}(x) = -\alpha \frac{b_S(x)x^2 + b_L(x)|x|^{3/2}}{b_S(x)|x|^{1/2} + b_L(x)|x|^{-1/2}}, \tag{1}$$

where α is a shape constant, $b_S(x)$ and $b_L(x)$ satisfy the following asymptotic formulas

$$\begin{array}{l} b_S(x) \to 0,\ b_L(x) \to 1 \text{ at } x \to 0, \\ b_S(x) \to 1,\ b_L(x) \to 0 \text{ at } x \gg 1. \end{array} \tag{2}$$

Note that the 3D dendrite tip shape (1) contains limiting transitions to previous theories. So, if $x \to 0$, $z_{\mathrm{AG}}(x) \to -x^2$ (Ivantsov parabola [4]). From the other hand, if $x \gg 1$, $z_{\mathrm{AG}}(x) \to -|x|^{3/2}$ (Plapp and Karma asymptotic shape [42]). The stitching functions $b_S(x)$ and $b_L(x)$ satisfying the asymptotic limiting conditions (2) can be selected in various ways. Here we chose them after Alexandrov and Galenko [36] in the form of

$$b_S(x) = \exp\left(-\frac{1}{x^{2k}}\right) \text{ and } b_L(x) = \exp\left(-x^{2k}\right) \tag{3}$$

with $k = 3$.

Next we submerge the dendrite tip shape (1) into a laminar flow of a viscous incompressible fluid coming towards the dendritic tip. The hydrodynamic model under consideration is given by conservation equations for mass (Equation (4)) and momentum (Equation (5))

$$\nabla \cdot \mathbf{V} = 0, \tag{4}$$

$$\rho\left(\frac{\partial \mathbf{V}}{\partial t} + (\mathbf{V}\cdot\nabla)\mathbf{V}\right) = -\nabla P + \nabla(2\mu S). \tag{5}$$

Here t is the time, $\mathbf{V}$ is the velocity vector, ρ is the constant density of fluid, P is the pressure, $2\mu S$ is the tensor of viscous stresses, S is the tensor of deformation rates, and μ is the coefficient of dynamic viscosity. We consider the succinonitrile melt as a Newtonian fluid, which means the constant dynamic viscosity μ.

A 3D computational domain is considered to simulate the flow around the dendrite tip using Equations (4) and (5) (see Figure 1). At the left domain boundary, a uniform fluid flow orthogonal to the boundary with constant velocity V_{in} is set. At all other domain boundaries (highlighted in dark grey), the boundary condition is defined by a zero pressure gradient. The light grey boundary sets an impermeable dendrite interface and is defined by the corresponding "no-slip" condition, where the fluid velocity at the boundary is zero. The dendrite shape (light grey colour) is determined by the Equation (1) with a tip radius R, and the angle at which the incoming flow passes around the dendrite tip is determined by the value of φ. The goals of the simulations are to determine the fluid current lines around the dendrite tip and the shear stress on the dendrite surface, which defines its growth characteristics. Simulations were performed using the FlowVision computational software for a succinonitrile melt with the parameters given in Table 1.

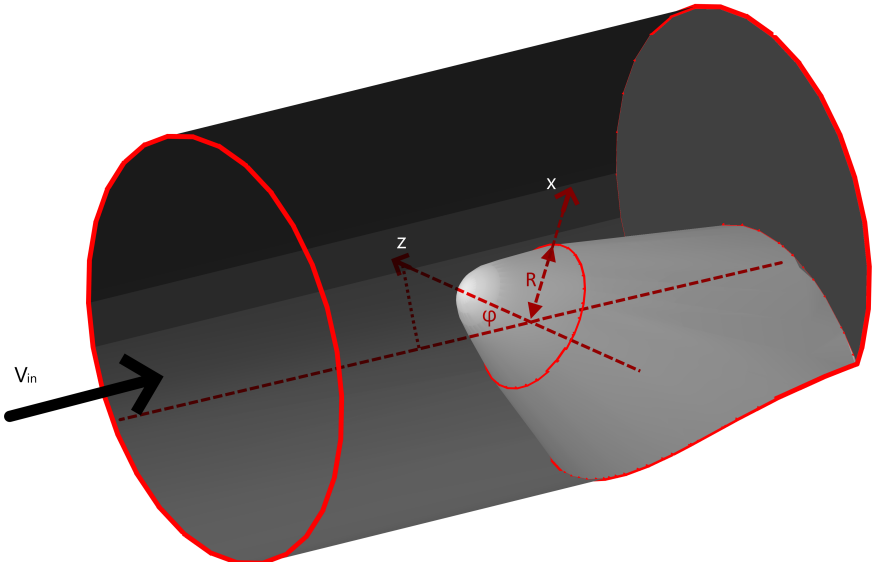

Figure 1. A computational domain (dark) around the dendrite tip (light grey).

Table 1. Parameters of the model for succinonitrile [43].

Parameter	Value	Unit
ρ	982	kg/m^3
μ	0.00264	Pa s
R	0.00015	m
V_{in}	1	m/s
φ	0; 30; 60; 90	grad
α	1	-

3. Results

The dendrite tip was placed in a viscous fluid flow tilted to 0, 30, 60, and 90 degrees to the dendrite axis. The results of our computer simulations are shown in Figures 2–5. In these illustrations, we show current lines in the liquid part of the system (the colour scale of fluid flow rate is shown on the left), while the shear stress is shown on the dendrite (the colour scale of shear stress is shown on the right). First of all, we note that the flow pattern around the dendrite changes drastically with a change in the flow slope. Thus, in the case of zero flow slope (Figure 2), a symmetrical flow pattern is expected, with a thin low-velocity layer, which is formed due to the no-slip condition at the boundary. A

flow tilt of 30 degrees produces low-velocity regions in front of and behind the dendrite (Figure 3). When the tilt angle is increased to 60 degrees, a wide stagnation zone occurs behind the dendrite (Figure 4). As this takes place, the shear stress in the front (red colour) and the back (blue colour) regions of the streamlined dendrite surface can differ by a factor of about 10. This effect is found at flow angles of 30, 60, and 90 degrees (see Figures 3–5), i.e., it is quite typical for different inclined flows. Note that in Figure 5 there are fluid flows behind the dendrite that come from the right boundary. This is explained by the fact that the incoming flow passing around the dendrite draws the melt located on dendrite's back side. Thus, a drop in pressure occurs there and the melt begins to flow into the area behind the dendrite from the right boundary. The model under consideration assumes a single dendrite with undisturbed liquid around it. In the case of many closely spaced dendrites, the influence of the boundaries can be much more complex and unpredictable.

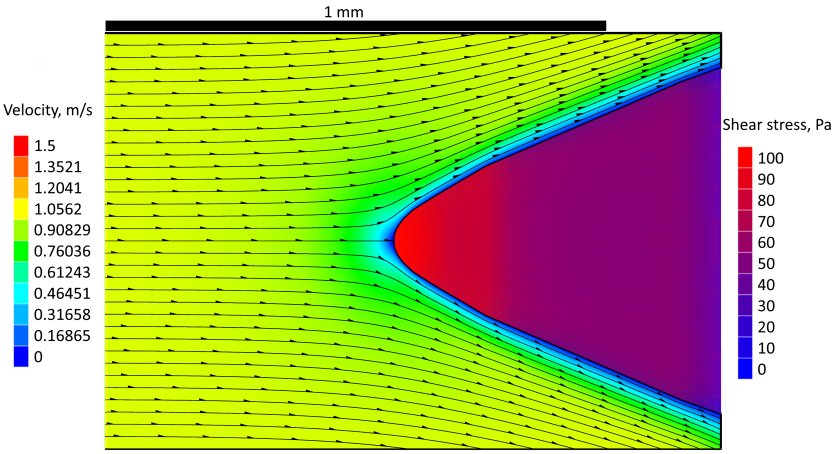

Figure 2. The velocity contour plot and streamlines for the melt area and the shear stress contour plot for the dendrite tip area. The fluid flow has a 0-degree slope to the dendrite axis.

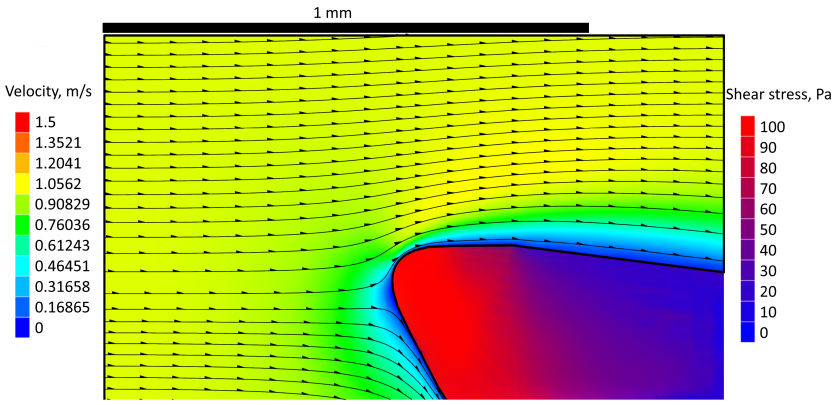

Figure 3. The velocity contour plot and streamlines for the melt area and the shear stress contour plot for the dendrite tip area. The fluid flow has a 30-degree slope to the dendrite axis.

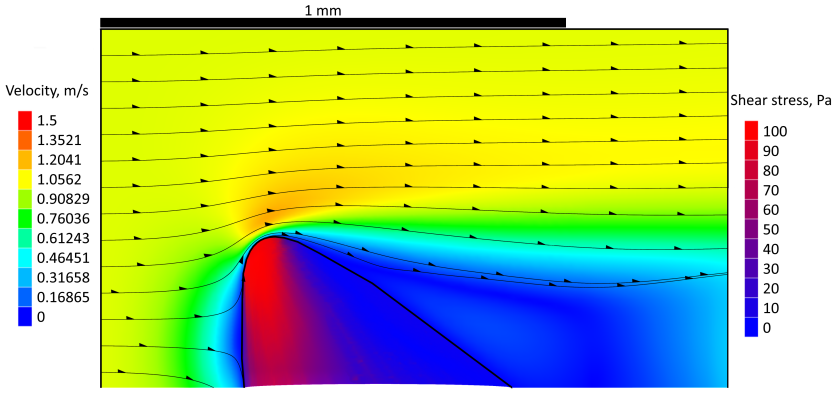

Figure 4. The velocity contour plot and streamlines for melt area and the shear stress contour plot for the dendrite tip area. The fluid flow has a 60-degree slope to the dendrite axis.

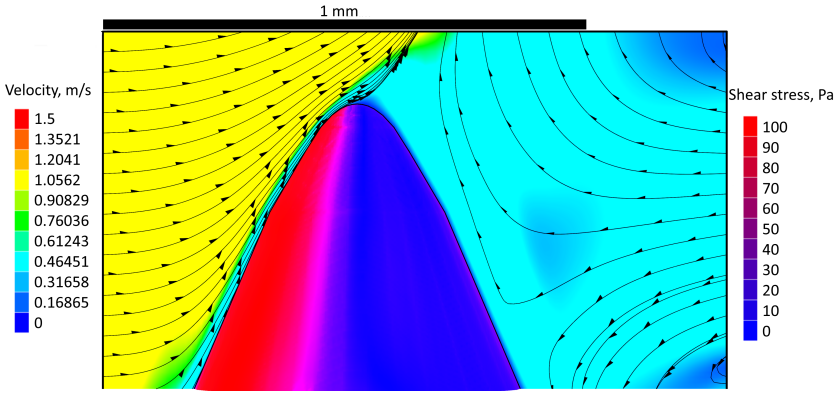

Figure 5. The velocity contour plot and streamlines for melt area and the shear stress contour plot for the dendrite tip area. The fluid flow has a 90-degree slope to the dendrite axis.

A boundary layer around the dendrite tip is almost a blue thin (low speed) layer for a 0, 30, and 60-degree fluid slopes, as shown in Figures 2–4. When paying our attention to Figure 5, we see that an intense fluid current along the dendrite surface (turquoise colour in upstream area) appears for a 90-degree flow slope. At the same time, the current in the area behind the dendrite (downstream area) is considerably weaker or may be absent altogether. The more intense flow in the anterior region (left in Figure 5) compared to the much less intense flow in the posterior region (right in Figure 5) may indicate different heat and mass transfer mechanisms in these regions. It is well known that at strong currents, the heat (J_h) and impurity (J_i) fluxes at the boundary are determined by the difference between the temperatures (impurity concentrations) at the boundary and away from it (instead of classic Fick's laws) [31–35], i.e.,

$$J_h = \alpha_h \rho c u_* (T_b - T_\infty), \; J_i = \alpha_i u_* (C_b - C_\infty), \tag{6}$$

where α_h and α_i represent the heat and mass (impurity) transfer coefficients, c is the specific heat of water, u_* is the friction velocity, and T_b (C_b) and T_∞ (C_∞) are the temperatures (impurity concentrations) at the dendrite boundary and away from it. Note that the ratio of coefficients α_h and α_i is defined by the diffusion coefficients for heat D_h and impurity D_i at that $\alpha_h/\alpha_i = (D_h/D_i)^l$ [34] with $2/3 < l < 4/5$ [44,45]. The friction velocity u_*, describing the flow at the solid–liquid boundary, is characterized through the shear stress τ and liquid density ρ [46] as $u_* = \sqrt{\tau/\rho}$. In the case of a 90-degree slope (Figure 5), $\tau \approx 10^2$ Pa at the front of the stream and $u_* \approx 0.3$ m s^{-1}. Therefore, the Reynolds number $\Re = u_* \mathrm{R} \rho / \mu \approx 17$; the system parameters here are taken from Table 1. It is significant to note that "purely laminar flow only exists up to $\Re = 10$" when dealing with an object in liquid stream [47]. In other words, a transition from laminar to turbulent currents on the upstream side of

the dendrite may occur. If this does happen, different heat and mass balance boundary conditions on the upstream and downstream sides of a growing dendritic crystal must be used.

An important point is that the theory developed by Ivantsov [48,49], Brener [50,51], Almgren, Dai and Hakim [52], Plapp and Karma [42], and recently generalized by Alexandrov and Galenko [36] predicts one universal dendritic tip shape no matter what undercooling is imposed. Namely, the dendrite shape is represented by parabola at the tip region (Formula (1), which transforms to parabola at $x \to 0$). When moving away from the vertex of the parabola at a distance of the order of a few tip diameters, Formula (1) works. Physically, this tip shape is controlled by the anisotropy of the surface energy. Other surface shapes that are possible in nature (flat, spherical, ellipsoidal, faceted, etc.) arise from variations in the initial conditions of pattern formation. However, if a dendritic pattern is formed, after a certain time, it reaches the steady-state growth mode, and its tip shape is described by the universal law (1). This means that the numerical simulations carried out in this paper for an inclined hydrodynamic stream flowing onto a dendritic tip with the shape (1) describe a wide class of dendritic crystals.

4. Conclusions

In summary, we have presented the results of numerical simulations concerning the influence of inclined fluid stream on the hydrodynamic flow around a dendritic crystal. As this takes place, the tip shape of dendrite is chosen according to the recently developed theory [36], which is confirmed by computer simulations and a large number of experimental data [37,38]. Our computer calculations have shown that inclined flow can have a significant effect on dendritic growth. First of all, on the downstream side of the dendrite low-velocity (stagnation) regions appear, where the shear stress is much smaller than on the upstream side. As this takes place, the greater the flow angle to the dendrite growth axis, the stronger the role of this effect is. At high attack angles there is an intense fluid flow in a narrow boundary layer on the upstream side of the dendrite. Our estimates show that the Reynolds number in this boundary layer for succinonitrile crystals is approximately 17 while "purely laminar flow only exists up to $\Re = 10$" when dealing with an object in liquid stream [47]. This means that the laminar-turbulent transition may occur on the upstream side of the dendrite. This in turn means that different heat and mass transfer mechanisms take place on the upstream and downstream sides of a dendritic crystal.

Thus, our simulations indicate the need for a more detailed study of inclined flow on crystal growth in the following directions.

(i) A numerical simulation of dendritic growth in an inclined liquid flow should be carried out, taking into account the conductive and convective heat and mass transfer on various (with respect to the flow) sides of the dendrite. Such simulations can be done using a direct solution of the heat and mass transfer problem with flow (e.g., the phase-field or enthalpy methods) [53–56], as well as using the convective boundary integral equation [57–59];

(ii) Intense convective currents on the upstream side of the dendrite are a potential source of morphological instability on its surface. It is therefore necessary to study the surface stability of the dendrite crystal to small morphological perturbations on its upstream side. Such a study should be done by following Refs. [60–63], who developed methods to study the stability induced by fluid currents;

(iii) In future computer simulations in the presence of inclined fluid flow, the real dendritic crystal morphology (e.g., taken from experiments) should be taken into account with allowance for secondary and tertiary branches. Here it is also important to perform simulations of the growth of several dendrites with overlapping branches and to consider the possibility of crystal nucleation ahead of the dendrites, i.e., to study crystallization with a nonequilibrium two-phase region in the presence of convective flow. Such computer simulations should be performed using directional and bulk solidification theories (see, among others, Refs. [64–70]).

Author Contributions: Conceptualization, I.O.S. and D.V.A.; methodology, D.V.A.; software, I.O.S. and E.V.P.; formal analysis, I.O.S., E.A.T., E.V.P., and D.V.A.; investigation, I.O.S., E.A.T., E.V.P., and D.V.A.; resources, I.O.S.; data curation, I.O.S. and E.V.P.; writing—original draft preparation, I.O.S., E.A.T., E.V.P., and D.V.A.; writing—review and editing, I.O.S., E.A.T., E.V.P., and D.V.A.; visualization, I.O.S. and E.V.P.; supervision, D.V.A.; project administration, E.A.T. and D.V.A.; funding acquisition, I.O.S. and D.V.A. All authors have read and agreed to the published version of the manuscript.

Funding: The research funding from the Ministry of Science and Higher Education of the Russian Federation (Ural Federal University Program of Development within the Priority-2030 Program) is gratefully acknowledged.

Data Availability Statement: All data generated or analysed during this study are included in this published article.

Acknowledgments: The authors express their heartfelt gratitude to Peter K. Galenko for his professional consultation and friendly support of this study. Numerical calculations were performed using the supercomputer 'URAN' of IMM UB RAS, Ekaterinburg, Russia.

Conflicts of Interest: The authors declare no conflict of interest.

References

1. Herlach, D.; Galenko, P.; Holland-Moritz, D. *Metastable Solids from Undercooled Melts*; Elsevier: Amsterdam, The Netherlands, 2007.
2. Alexandrov, D.V.; Galenko, P.K. A review on the theory of stable dendritic growth. *Philos. Trans. R. Soc. A* **2021**, *379*, 20200325. [CrossRef] [PubMed]
3. Alexandrov, D.V.; Titova, E.A.; Galenko, P.K.; Rettenmayr, M.; Toropova, L.V. Dendrite tips as elliptical paraboloids. *J. Phys. Condens. Matter* **2021**, *33*, 443002. [CrossRef] [PubMed]
4. Alexandrov, D.V.; Galenko, P.K. Dendrite growth under forced convection: Analysis methods and experimental tests. *Physics-Uspekhi* **2014**, *57*, 771–786. [CrossRef]
5. Kurz, W.; Rappaz, M.; Trivedi, R. Progress in modelling solidification microstructures in metals and alloys. Part II: Dendrites from 2001 to 2018. *Int. Mater. Rev.* **2021**, *66*, 30–76. [CrossRef]
6. Kurz, W.; Fisher, D.J.; Trivedi, R. Progress in modelling solidification microstructures in metals and alloys: Dendrites and cells from 1700 to 2000. *Int. Mater. Rev.* **2019**, *64*, 311–354. [CrossRef]
7. Asta, M.; Beckermann, C.; Karma, A.; Kurz, W.; Napolitano, R.; Plapp, M.; Purdy, G.; Rappaz, M.; Trivedi, R. Solidification microstructures and solid-state parallels: Recent developments, future directions. *Acta Mater.* **2009**, *57*, 941–971. [CrossRef]
8. Alexandrov, D.V.; Galenko, P.K. Dendritic growth with the six-fold symmetry: Theoretical predictions and experimental verification. *J. Phys. Chem. Solids* **2017**, *108*, 98–103. [CrossRef]
9. Eckler, K.; Herlach, D.M. Measurements of dendrite growth velocities in undercooled pure Ni-melts—Some new results. *Mater. Sci. Eng. A* **1994**, *178*, 159–162. [CrossRef]
10. Galenko, P.K.; Funke, O.; Wang, J.; Herlach, D.M. Kinetics of dendrities growth under the influence of convective flow in solidification of undercooling droplets. *Mater. Sci. Eng. A* **2004**, *375–377*, 488–492. [CrossRef]
11. Funke, O.; Phanikumar, G.; Galenko, P.K.; Chernova, L.; Reutzel, S.; Kolbe, M.; Herlach, D.M. Dendrite growth velocity in levitated undercooled nickel melts. *J. Cryst. Growth* **2006**, *297*, 211–222. [CrossRef]
12. Alexandrov, D.V.; Galenko, P.K. Thermo-solutal and kinetic regimes of an anisotropic dendrite growing under forced convective flow. *Phys. Chem. Chem. Phys.* **2015**, *17*, 19149–19161. [CrossRef] [PubMed]
13. Kao, A.; Toropova, L.V.; Krastins, I.; Demange, G.; Alexandrov, D.V.; Galenko, P.K. A stable dendritic growth with forced convection: A test of theory using enthalpy-based modeling methods. *JOM* **2020**, *72*, 3123–3131 [CrossRef]
14. Glicksman, M.E.; Koss, M.B. Dendritic growth velocities in microgravity. *Phys. Rev. Lett.* **1994**, *73*, 573–576. [CrossRef]
15. Bouissou, P.; Pelcé P. Effect of a forced flow on dendritic growth. *Phys. Rev. A* **1989**, *40*, 6637–6680. [CrossRef]
16. Gibbs, J.W.; Mohan, K.A.; Gulsoy, E.B.; Shahani, A.J.; Xiao, X.; Bouman, C.A.; De Graef, M.; Voorhees, P.W. The three-dimensional morphology of growing dendrites. *Sci. Rep.* **2015**, *5*, 11824. [CrossRef] [PubMed]
17. Galenko, P.K.; Reuther, K.; Kazak, O.V.; Alexandrov, D.V.; Rettenmayr, M. Effect of convective transport on dendritic crystal growth from pure and alloy melts. *Appl. Phys. Lett.* **2017**, *111*, 031602. [CrossRef]
18. Mathiesen, R.H.; Arnberg, L.; Bleuet, P.; Somogyi, A. Crystal fragmentation and columnar-to-equiaxed transitions in Al-Cu studied by synchrotron X-ray video microscopy. *Metall. Mater. Trans. A* **2006**, *37*, 2515–2524. [CrossRef]
19. Ruvalcaba, D.; Mathiesen, R.H.; Eskin, D.G.; Arnberg, L.; Katgerman, L. In situ observations of dendritic fragmentation due to local solute-enrichment during directional solidification of an aluminum alloy. *Acta Mater.* **2007**, *55*, 4287–4292. [CrossRef]
20. Ramirez, J.C.; Beckermann, C. Examination of binary alloy free dendritic growth theories with a phase-field model. *Acta Mater.* **2005**, *53*, 1721–1736. [CrossRef]
21. Tong, X.; Beckermann, C.; Karma, A.; Li, Q. Phase-field simulations of dendritic crystal growth in a forced flow. *Phys. Rev. E* **2001**, *63*, 061601. [CrossRef]

22. Jeong, J.-H.; Goldenfeld, N.; Dantzig, J.A. Phase field model for three-dimensional dendritic growth with fluid flow. *Phys. Rev. E* **2001**, *64*, 041602. [CrossRef] [PubMed]
23. Bouissou, P.; Perrin, B.; Tabeling, P. Influence of an external flow on dendritic crystal growth. *Phys. Rev. A* **1989**, *40*, 509–512. [CrossRef] [PubMed]
24. Buchholz, A.; Engler, S. The influence of forced convection on solidification interfaces. *Comp. Mater. Sci.* **1996**, *7*, 221–227. [CrossRef]
25. Zhongming, R.; Junze, J.; Keren, G. Effect of fluid flow on dendritic structure of Al-Si alloy. *J. Mater. Sci.* **1991**, *26*, 3599–3602. [CrossRef]
26. Hyers, R.W.; Matson, D.M.; Kelton, K.F.; Rogers, J.R. Convection in containerless processing. *Ann. N. Y. Acad. Sci.* **2004**, *1027*, 474–494. [CrossRef]
27. Matson, D.M.; Hyers, R.W.; Volkmann, T. Peritectic alloy rapid solidification with electromagnetic convection. *J. Jpn. Soc. Microgravity Appl.* **2010**, *27*, 238–244.
28. Herlach, D.M. (Ed.) *Phase Transformations in Multicomponent Melts*; Wiley-VCH: Weinheim, Germany, 2008; p. 353
29. Herlach, D.M.; Galenko, P.K. Rapid solidification: In situ diagnostics and theoretical modelling. *Mater. Sci. Eng. A* **2007**, *449–451*, 34–41. [CrossRef]
30. Alexandrov, D.V.; Toropova, L.V. The role of incoming flow on crystallization of undercooled liquids with a two-phase layer. *Sci. Rep.* **2022**, *12*, 17857. [CrossRef]
31. Toropova, L.V.; Galenko, P.K.; Alexandrov, D.V. A stable mode of dendritic growth in cases of conductive and convective heat and mass transfer. *Crystals* **2022**, 12, 965. [CrossRef]
32. Toropova, L.V.; Alexandrov, D.V.; Galenko, P.K. Convective and conductive selection criteria of a stable dendritic growth and their stitching. *Math. Meth. Appl. Sci.* **2021**, 44, 12139–12151. [CrossRef]
33. Notz, D.; McPhee, M.G.; Worster, M.G.; Maykut, G.A.; Schlünzen, K.H.; Eicken, H. Impact of underwater-ice evolution on Arctic summer sea ice. *J. Geophys. Res.* **2003**, *108*, 3223. [CrossRef]
34. McPhee, M.G.; Maykut, G.A.; Morison, J.H. Dynamics and thermodynamics of the ice/upper ocean system in the marginal ice zone of the Greenland sea. *J. Geophys. Res.* **1987**, *92*, 7017. [CrossRef]
35. Alexandrov, D.V.; Nizovtseva, I.G. To the theory of underwater ice evolution, or nonlinear dynamics of "false bottoms". *Int. J. Heat Mass Trans.* **2008**, *51*, 5204–5208. [CrossRef]
36. Alexandrov, D.V.; Galenko, P.K. The shape of dendritic tips. *Philos. Trans. R. Soc. A* **2020**, *378*, 20190243. [CrossRef] [PubMed]
37. Alexandrov, D.V.; Toropova, L.V.; Titova, E.A.; Kao, A.; Demange, G.; Galenko, P.K.; Rettenmayr, M. The shape of dendritic tips: A test of theory with computations and experiments. *Philos. Trans. R. Soc. A* **2021**, *379*, 20200326. [CrossRef] [PubMed]
38. Toropova, L.V. Shape functions for dendrite tips of SCN and Si. *Eur. Phys. J. Spec. Top.* **2022**, *231*, 1129–1133. [CrossRef]
39. Huang, S.-C.; Glicksman, M.E. Overview 12: Fundamentals of dendritic solidification—I. Steady-state tip growth. *Acta Metall.* **1981**, *29*, 701–715. [CrossRef]
40. Bisang, U.; Bilgram, J.H. Shape of the tip and the formation of sidebranches of xenon dendrites. *Phys. Rev. Lett.* **1995**, *75*, 3898–3901. [CrossRef]
41. Titova, E.A.; Galenko, P.K.; Alexandrov, D.V. Method of evaluation for the non-stationary period of primary dendritic crystallization. *J. Phys. Chem. Solids* **2019**, *134*, 176–181. [CrossRef]
42. Plapp, M.; Karma, A. Multiscale random-walk algorithm for simulating interfacial pattern formation. *Phys. Rev. Lett.* **2000**, *84*, 1740–1743. [CrossRef]
43. Gao, J.; Han, M.; Kao, A.; Pericleous, K.; Alexandrov, D.V.; Galenko P.K. Dendritic growth velocities in an undercooled melt of pure nickel under static magnetic fields: A test of theory with convection. *Acta Mat.* **2016**, *103*, 184–191. [CrossRef]
44. Owen, P.R.; Thomson,W.R. Heat transfer across rough surfaces. *J. Fluid Mech.* **1963**, *15*, 321–334. [CrossRef]
45. Yaglom, A.M.; Kader, B.A. Heat and mass transfer between a rough wall and turbulent flow at high Reynolds and Peclet numbers. *J. Fluid Mech.* **1974**, *62*, 601–623. [CrossRef]
46. Tritton, D.J. *Physical Fluid Dynamics*; Clarendon Press: Oxford, UK, 1988.
47. Wikipedia. Available online: https://en.wikipedia.org/wiki/Reynolds$_$number (accessed on 1 November 2022).
48. Ivantsov, G.P. Temperature field around spherical, cylinder and needle-like dendrite growing in supercooled melt. *Dokl. Akad. Nauk SSSR* **1947**, *58*, 567–569.
49. Ivantsov, G.P. On a growth of spherical and needle-like crystals of a binary alloy. *Dokl. Akad. Nauk SSSR* **1952**, *83*, 573–575.
50. Brener, E. Needle-crystal solution in three-dimensional dendritic growth. *Phys. Rev. Lett.* **1993**, *71*, 3653–3656. [CrossRef]
51. Brener, E. Pattern formation in three-dimensional dendritic growth. *Physica A* **1999**, *263*, 338–344. [CrossRef]
52. Almgren, R.; Dai, W.-S.; Hakim, V. Scaling behavior in anisotropic Hele-Shaw flow. *Phys. Rev. Lett.* **1993**, *71*, 3461–3464. [CrossRef]
53. Toropova, L.V.; Galenko, P.K.; Alexandrov, D.V.; Rettenmayr, M.; Kao, A.; Demange, G. Non-axisymmetric growth of dendrite with arbitrary symmetry in two and three dimensions: Sharp interface model vs. phase-field model. *Eur. Phys. J. Spec. Top.* **2020**, *229*, 2899–2909. [CrossRef]
54. Kao, A.; Toropova, L.V.; Alexandrov, D.V.; Demange, G.; Galenko, P.K. Modeling of dendrite growth from undercooled nickel melt: Sharp interface model versus enthalpy method. *J. Phys. Condens. Matter* **2020**, *32*, 194002. [CrossRef]
55. Demange, G.; Zapolsky, H.; Patte, R.; Brunel, M. Growth kinetics and morphology of snowflakes in supersaturated atmosphere using a three-dimensional phase-field model. *Phys. Rev. E* **2017**, *96*, 022803. [CrossRef] [PubMed]

56. Gao, J.; Kao, A.; Bojarevics, V.; Pericleous, K.; Galenko, P.K.; Alexandrov, D.V. Modeling of convection, temperature distribution and dendritic growth in glass-fluxed nickel melts. *J. Cryst. Growth* **2017**, *471*, 66–72. [CrossRef]
57. Saville, D.A.; Beaghton, P.J. Growth of needle-shaped crystals in the presence of convection. *Phys. Rev. A* **1988**, *37*, 3423–3430. [CrossRef] [PubMed]
58. Titova, E.A.; Alexandrov, D.V. Analysis of the boundary integral equation for the growth of a parabolic/paraboloidal dendrite with convection. *J. Phys. Condens. Matter* **2022**, *34*, 244002. [CrossRef] [PubMed]
59. Titova, E.A.; Alexandrov, D.V. The boundary integral equation for curved solid/liquid interfaces propagating into a binary liquid with convection. *J. Phys. A Math. Theor.* **2022**, *55*, 055701. [CrossRef]
60. Chiareli, A.O.P.; Worster, M.G. Flow focusing instability in a solidifying mushy layer. *J. Fluid Mech.* **1995**, *297*, 293–305. [CrossRef]
61. Feltham, D.L.; Worster, M.G. Flow-induced morphological instability of a mushy layer. *J. Fluid Mech.* **1999**, *391*, 337–357. [CrossRef]
62. Alexandrov, D.V.; Malygin, A.P. Convective instability of directional crystallization in a forced flow: The role of brine channels in a mushy layer on nonlinear dynamics of binary systems. *Int. J. Heat Mass Trans.* **2011**, *54*, 1144–1149. [CrossRef]
63. Alexandrov, D.V.; Malygin, A.P. Flow-induced morphological instability and solidification with the slurry and mushy layers in the presence of convection. *Int. J. Heat Mass Trans.* **2012**, *55*, 3196–3204. [CrossRef]
64. Galenko, P.K.; Zhuravlev, V.A. *Physics of Dendrites*; World Scientific: Singapore, 1994.
65. Worster, M.G. Convection in mushy layers. *Ann. Rev. Fluid Mech.* **1997**, *29*, 91–122. [CrossRef]
66. Kessler, D.A.; Koplik, J.; Levine, H. Pattern selection in fingered growth phenomena. *Adv. Phys.* **1988**, *37*, 255–339. [CrossRef]
67. Brener, E.A.; Mel'nikov, V.I. Pattern selection in two-dimensional dendritic growth. *Adv. Phys.* **1991**, *40*, 53–97. [CrossRef]
68. Toropova, L.V.; Alexandrov, D.V. Dynamical law of the phase interface motion in the presence of crystals nucleation. *Sci. Rep.* **2022**, *12*, 10997. [CrossRef] [PubMed]
69. Makoveeva, E.V.; Alexandrov, D.V. Mathematical simulation of the crystal nucleation and growth at the intermediate stage of a phase transition. *Russ. Metall. (Metally)* **2018**, *2018*, 707–715. [CrossRef]
70. Makoveeva, E.; Alexandrov, D.; Ivanov, A. Mathematical modeling of crystallization process from a supercooled binary melt. *Math. Meth. Appl. Sci.* **2021**, *44*, 12244–12251. [CrossRef]